Laser-induced continuum structure in the two ionization continua of xenon

K. Böhmer, T. Halfmann, L. P. Yatsenko,* D. Charalambidis,† A. Horsmans, and K. Bergmann
Fachbereich Physik der Universität, 67653 Kaiserslautern, Germany
(Received 15 November 2001; published 19 July 2002)

We report the observation of pronounced, spectrally narrow laser-induced continuum structures (LICS) in the two ionization continua of xenon. A nanosecond laser pulse with nearly transform-limited bandwidth induces a LICS by coupling the initially unpopulated $5p^5\,9p[1/2]_0$ state to the continuum. The LICS is probed by one-photon ionization of the $5p^5\,6p[1/2]_0$ state. This state is populated in an independent excitation step by an additional laser pulse acting prior to the probe and dressing pulses. The two ionization channels that leave the xenon ion in either the $^2P_{1/2}$ or the $^2P_{3/2}$ fine-structure state are detected separately by monitoring the kinetic energy of the photoelectrons in a time-of-flight electron spectrometer. A suppression of the photoelectron signal of up to 80% as compared to the far off resonance value is achieved. The line shapes reveal a Fano parameter close to zero. The LICS is identical for the coupling into the two continua. Therefore the branching ratio into the two ionization channels does not vary with the dressing-laser detuning for the coupling scheme implemented here.

DOI: 10.1103/PhysRevA.66.013406 PACS number(s): 32.80.Qk, 32.80.Fb

I. INTRODUCTION

Continua of quantum systems have been traditionally considered as sinks. Once the system is excited into such a continuum it decays irreversibly, with a probability that is determined by its structure parameters. This view of continua has been radically revised in recent years. Coherent interactions of laser radiation with quantum systems reveal nonconventional decay characteristics, such as an enhanced or diminished decay rate. In the latter case the continuum does not behave as a sink. Coherence is induced within the continuum and population oscillates through it between bound states. Decay of the system is thus reduced or even prohibited through coherent trapping of the population in the bound part of the spectrum. A ''window'' or ''dark'' resonance appears in the decay spectrum.

Laser-induced continuum structure (LICS) [1,2] is one of the most interesting effects associated with the coupling of bound and continuum states by coherent radiation. In LICS a strong laser field (the dressing field) couples a bound state of an atomic or molecular system, that initially carries no population, to a continuum. In the dressed atom picture the bound state is thus embedded in the continuum. A second laser field (the probe field) couples another bound state of the system, which initially carries the population, to the same continuum. The decay to the continuum is modified by a quantum interference process between different pathways. Unless otherwise specified decay will refer to ionization in the present work. The ionization rate as a function of the wavelength of one of the laser fields shows a resonance structure that may exhibit a maximum and/or a minimum depending on whether the interference is constructive or destructive at the specific wavelength interval.

The existence of the LICS phenomenon has been predicted in the 70s by Heller and Popov [3]. As the LICS scheme involves two bound states coupled to each other and to the continuum it resembles the process of autoionization, although the type of the couplings differs in the two processes. The first complete theoretical treatment of the process that took into account all the relevant couplings and has shown its equivalence to autoionization was by Bo-nian Dai and Lambropoulos [4]. The first experimental demonstrations of the effect used as probe the polarization rotation of the probing field [5] or third-harmonic generation [6]. Implementation of the most direct demonstration of the LICS, that is through ionization, took longer due to difficulties posed by other processes that may mask the effect. The first experiment attempting to demonstrate LICS in ionization was in Xe [7]. However, theoretical modeling [8] of this experiment predicted results that are different than those presented in Ref. [7]. Later two successful experiments in the smooth (unstructured) one-electron continuum of Na [9] have shown slightly asymmetric LICS structures. Improvement in the experiments led to the measurement of high-contrast LICS resonances in alkaline atoms [10]. In all these measurements the observed asymmetry of the LICS line shape was not strongly pronounced. An enhancement of ionization was the predominant feature of the resonances. The most spectacular demonstration of the effect of LICS in a smooth continuum was in He [11,12], where very pronounced spectrally narrow LICS features exhibiting both ionization maxima and minima have been reported and investigated with respect to various parameters of the two electromagnetic fields. In that work, both bound states of the LICS scheme were excited states. One of those states was initially populated by electron impact in a pulsed supersonic beam of helium, involving an electron-seeded electric discharge [13]. In that work, a reduction of ionization by up to 70% due to coherent population trapping was observed. This is the strongest ionization suppression ever observed in this type of experiments.

*Permanent address: Institute of Physics, Ukrainian Academy of Sciences, prospect Nauki 46, Kiev-22, 03650, Ukraine.

†Permanent address: Foundation for Research and Technology—Hellas, Institute of Electronic Structure and Laser, P.O. Box 1527, Heraklion, 711 10 Crete, Greece and Department of Physics, University of Crete, P.O. Box 2208, Heraklion, 710 03 Crete, Greece.

Closely related investigations of the LICS in the structured continua of two valence electron systems, that is, in the vicinity of autoionizing states, resulted in further pronounced structures in Ca [14] and Mg [15] which were controllable through the field parameters. In the latter case, which consists of a ladder ionization scheme including two strongly coupled autoionizing states, the possibility of stabilization of ionization at increased coupling intensities was demonstrated. Extension of LICS into the ionization continuum of molecules has been recently achieved in the NO molecule [16].

Brumer and Shapiro taking advantage of the possibility of modifying continua through LICS have suggested an approach based on the LICS, towards control of products of the interaction of laser radiation with matter [17]. The idea behind this approach is that if the decay is in multiple continua the induced structure will be in general different for each continuum, as it depends on the specific properties of it. Thus the branching into the different continua may become strongly wavelength dependent and consequently controllable. In Ref. [17] dissociative continua have been considered, leading to the control of dissociation branching ratios, which is directly related to the important control of chemical reactions. This suggestion has been experimentally confirmed in Na_2 [18]. The method has further been implemented in multiple electronic continua of atoms by Cavalieri *et al.* [19]. In this experimental work the modification of the two spin-orbit ionization continua $^2P_{1/2}$ and $^2P_{3/2}$ of Xe through LICS has been reported, utilizing high-resolution photoelectron spectroscopy. Control of the ionization branching on a 10% order of magnitude has been demonstrated.

In the experiment of Ref. [19] the probing was done by three-photon excitation to both continua from the ground state of Xe. The use of multiphoton excitation leads to the coupling of multiple angular momentum continua, some of which do not contribute to the quantum interference. Therefore an increased background signal originates from these incoherent channels, and the dynamic range of the induced structure is diminished. Relying on the experience from the very pronounced feature observed in the He experiment [11,12], LICS in the two ionization continua of Xe is studied in the present work utilizing almost transform-limited laser pulses and the coupling scheme shown in Fig. 1. The $5p^5\,6p[1/2]_0$ and the $5p^5\,9p[1/2]_0$ atomic Xe states are coupled to the same continua through two laser fields. The $5p^5\,6p[1/2]_0$ state is populated from the ground state by a two-photon process. The aim of this study is to explore the possibility of generating pronounced LICS resonances in multiple continua, utilizing improved laser radiation and coupling scheme properties. Provided that pronounced LICS resonances are indeed possible to generate, the work is further aiming at the investigation of the possibility to improve the dynamic range of the control of the ionization branching ratio.

II. COUPLING SCHEME

The two ionization channels in xenon correspond to the two fine-structure states $^2P_{1/2}$ and $^2P_{3/2}$ of the ion core, separated by 1.3 eV in energy (see Fig. 1). In the present experiment photoionization into these channels is distinguished by measuring the kinetic energy of the photoelectrons. Moderate energy resolution suffices.

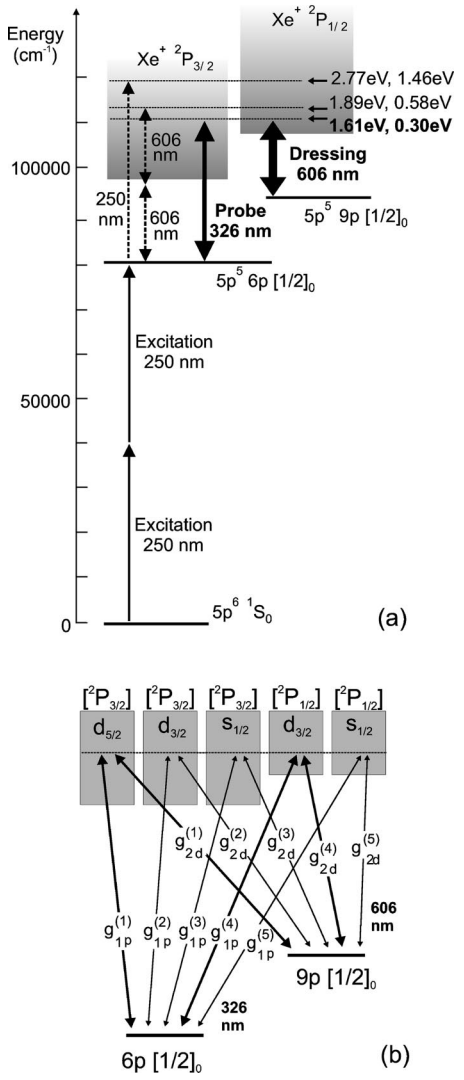

FIG. 1. (a) LICS coupling scheme in xenon. The $5p^5\,6p[1/2]_0$ state is excited from the ground state $5p^6\,{}^1S_0$ by two photons of 4.96 eV ($\lambda = 250$ nm). The dressing laser at 606 nm couples the $5p^5\,9p[1/2]_0$ state to the continuum states. The LICS is probed by one-photon ionization from the $5p^5\,6p[1/2]_0$ state at 326 nm. The process leading to the formation of LICS (with coincident probe and dressing pulses) is separated from the excitation process by a suitable time delay. The horizontal arrows indicate the kinetic energies of the photoelectrons in both ionization channels generated by the various laser pulses. (b) Details of the coupling scheme. Five continuum states are coupled to the bound states by linearly polarized laser fields. A theoretical estimate indicates that the couplings marked by heavy lines dominate the ionization process. The notation is $[^2P_{j_c}]l_j$, where j_c and j denote the angular momentum quantum numbers of the ion core and the electron, respectively.

In the simplest LICS coupling scheme a bound state (state 1), which carries the population initially, is coupled to the continuum states by one probe-laser photon. The continuum states are coupled to another, initially unpopulated, state

(state 2) by one photon of the dressing laser. This configuration avoids the use of radiation at wavelength $\lambda < 92.3$ nm which would be needed to couple the xenon ground state to the continuum with a one-photon process. Nonresonant multiphoton ionization with linearly polarized light would allow the use of longer wavelengths, but leads to the excitation of continuum states with a range of angular momentum quantum numbers l. Not all of these continuum states are coupled to state 2 by the dressing laser via a one-photon process. Therefore the maximum suppression of the ion signal is limited, as previous work has shown [19]. Resonantly enhanced multiphoton ionization via an intermediate state suffers from additional bound-bound couplings between state 1 and the ground state during the LICS process. In addition to the bound-continuum coupling of interest bound-bound transitions may occur.

In our experiment (see Fig. 1), we separate the excitation and the probe process with an appropriate time delay between the laser pulses. The $5p^5\,6p[1/2]_0$ state is excited from the ground state $5p^6\,{}^1S_0$ by two photons of 4.96 eV ($\lambda = 250$ nm). One probe-laser photon of 3.80 eV ($\lambda = 326$ nm) couples the $5p^5\,6p[1/2]_0$ state to the continuum. One dressing photon of 2.05 eV ($\lambda = 606$ nm) couples the $5p^5\,9p[1/2]_0$ state to the same continuum states. According to the selection rules the continuum states $[^2P_{3/2}]d_{5/2}$, $[^2P_{3/2}]d_{3/2}$, $[^2P_{3/2}]s_{1/2}$, $[^2P_{1/2}]d_{3/2}$, and $[^2P_{1/2}]s_{1/2}$ are excited. Here $[^2P_{j_c}]l_j$ is the jj coupling notation, where j_c and j denote the quantum numbers of the angular momentum of the ion core and the electron, respectively. All of them are coupled to the $5p^5\,9p[1/2]_0$ state by the dressing laser [see Fig. 1(b)].

The dynamics of the LICS process is described by the time-dependent Schrödinger equation that includes the atomic Hamiltonian and the interaction with the laser fields. In this formalism (described in detail in Refs. [2,12]) the wave function of the system is a superposition of bound and continuum states. After adiabatic elimination [2] of the nonresonant bound and continuum states one obtains the time-dependent Schrödinger equation for the amplitudes $C_i(t)$ of the bound states 1 and 2. Using the solution of this equation the total ionization probability is calculated.

In the case of multiple continua the branching ratio into different decay channels is of interest. The coupling between bound state i ($i=1,2$ for the $5p^5\,6p[1/2]_0$ and $5p^5\,9p[1/2]_0$ states) and continuum state α ($\alpha = 1, \ldots, 5$) is described by complex ionization amplitudes $g_{ij}^{(\alpha)}$, where $j = p,d$ denotes the probe- or dressing-laser field. The respective ionization rates are $\Gamma_{ij}^{(\alpha)} = |g_{ij}^{(\alpha)}|^2$. Extending the formalism used in Ref. [20] for two continua to the case of five continua, we derive the probability for exciting a continuum state with the ion in either a $^2P_{3/2}$ or a $^2P_{1/2}$ fine-structure level, corresponding to fast or slow electrons, respectively,

$$P_{P_{3/2}} = \int_{-\infty}^{\infty} dt \sum_{\alpha=1,2,3} |g_{1p}^{(\alpha)} C_1(t) + g_{2d}^{(\alpha)} C_2(t)|^2 + \int_{-\infty}^{\infty} dt \sum_{\alpha=1,2,3} |g_{2p}^{(\alpha)}|^2 |C_2(t)|^2 \qquad (1)$$

and

$$P_{P_{1/2}} = \int_{-\infty}^{\infty} dt \sum_{\alpha=4,5} |g_{1p}^{(\alpha)} C_1(t) + g_{2d}^{(\alpha)} C_2(t)|^2 + \int_{-\infty}^{\infty} dt \sum_{\alpha=4,5} |g_{2p}^{(\alpha)}|^2 |C_2(t)|^2. \qquad (2)$$

The amplitudes C_i of the bound states depend on the detuning of the probe- and dressing-laser frequencies from the two-photon resonance between states 1 and 2. It follows from equations 1 and 2 that the difference in the line shapes of the LICS in the individual channels—and therefore the possible extent of control—is determined by the value of the amplitudes $g_{ij}^{(\alpha)}$.

III. EXPERIMENT

A. Electron spectrometer

The population of the individual continuum channels is monitored by measuring the kinetic energy of the photoelectrons in a time-of-flight electron spectrometer using a parabolic electrostatic reflector [21,22]. This setup allows the separation of photoelectrons (kinetic energy 1.61 eV and 0.30 eV) generated by the absorption of one probe-laser photon, by the absorption of two photons from the dressing laser (kinetic energy 1.89 eV and 0.58 eV) or by the absorption of one photon from the excitation laser (kinetic energy 2.77 eV, 1.46 eV) (see Fig. 1). The intensity of the excitation laser is adjusted to maximize the population in the $5p^5\,6p[1/2]_0$ state after the interaction with the excitation laser. The two-photon ionization of state $5p^5\,6p[1/2]_0$ induced by the strong dressing laser yields a significant contribution to the total ion signal, as it is obvious from the electron spectra.

Xenon atoms are expanded from a stagnation region at room temperature and a pressure of typically 500 mbar through a pulsed nozzle (General Valve, opening diameter 0.8 mm). The resulting supersonic jet is collimated by a skimmer (orifice 0.8 mm), 132 mm downstream of the nozzle. The skimmer separates the source chamber from the interaction and detection region. The pulsed beam of xenon atoms is intersected by the lasers at right angle at a distance of 103 mm downstream from the skimmer. The particle density in the interaction region is estimated to be approximately 10^{13} atoms/cm^3.

The interaction region is located in the focus of an electrostatic parabolic mirror (see Fig. 2) formed by two nickel-coated stainless steel meshes separated by 2 mm. The photoelectrons generated in the field-free interaction region are reflected in the electric field between the two meshes [21,22]. After leaving the field-free region they are accelerated and travel along a time-of-flight segment at the end of which they are detected on a micro-sphere-plate (El Mul Technologies). The signal output of the micro-sphere-plate is amplified by fast broadband amplifiers and processed in boxcar gated integrators (EG&G 4121B). The energy resolution of the spectrometer is typically 150 meV at $E_{kin} = 4.4$ eV, which is sufficient to resolve photoelectrons from the two ionization continua of xenon. The detection efficiency depends on the

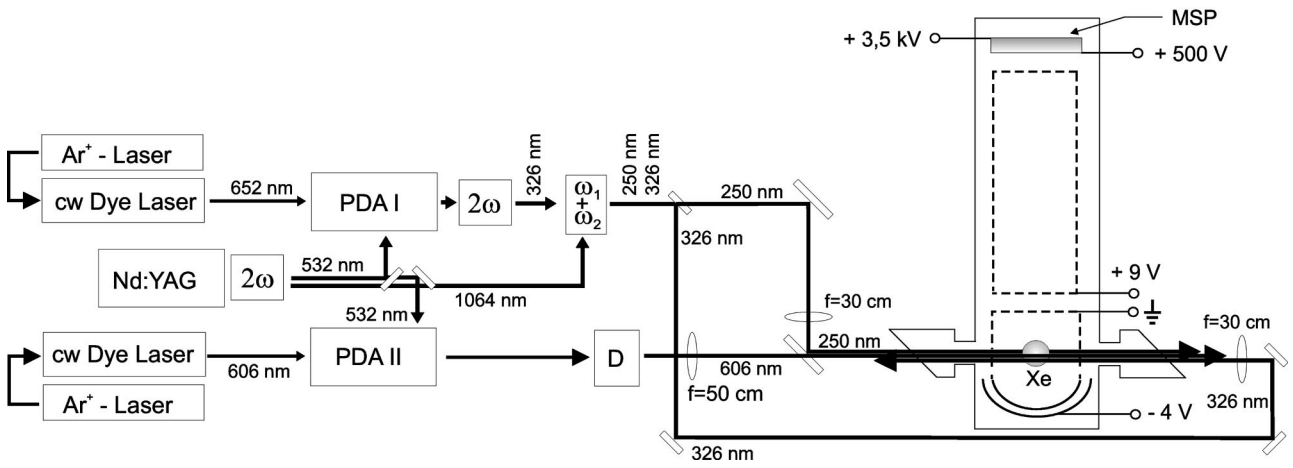

FIG. 2. The experimental setup showing the electron spectrometer and the laser system for the generation of pulses with nearly transform-limited bandwidth. Excitation of the $5p^5\,6p[1/2]_0$ level in xenon from the ground state $5p^6\,{}^1S_0$ requires two photons at 250 nm. This wavelength is generated by frequency doubling and sum-frequency mixing of the output from a pulsed dye amplifier, seeded by a tunable single-mode cw laser system. The residual radiation at 326 nm is used for the probe process. The output of a second pulsed dye amplifier provides the dressing-laser pulse at 606 nm. After the dressing-laser pulse passes an optical delay line (D), the three laser beams are focused into the atomic jet. The photoelectrons generated by the probe laser are reflected by an electrostatic parabolic mirror and, after passing a time-of-flight segment (length $l=1$ m), detected on a micro-sphere-plate. The energy resolution of the setup was typically 150 meV.

voltage between the two parabolic meshes and on the voltage between the meshes forming the acceleration region. The optimum values for these voltages depend on the electron energy. The slow and fast electrons are detected separately with the voltages set to their respective optimum values in order to maximize the detection efficiency. Figures 3(a) and 3(b) show the measured time-of-flight spectra for the fast and slow photoelectrons generated by probe-laser-induced ionization of the $5p^5\,6p[1/2]_0$ state.

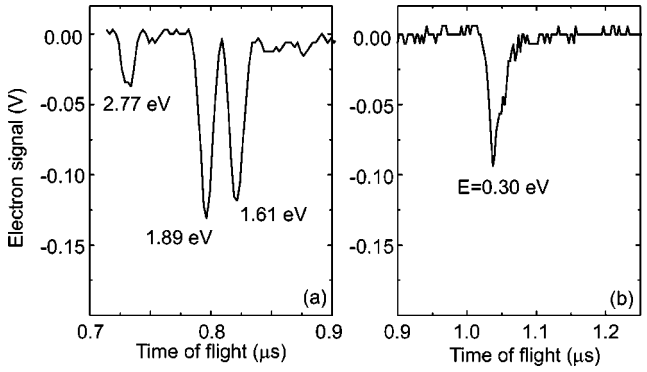

FIG. 3. Time-of-flight spectra of the photoelectrons. (a) Electron signals from the fast electrons in the ${}^2P_{3/2}$ channel generated by the various laser pulses. The voltage between the parabolic meshes is $U_p=-6.0$ V. The acceleration voltage is $U_a=3.6$ V. The acceleration voltage is reduced such that the 1.89 eV electrons produced by two dressing photons can be resolved from the 1.61 eV electrons generated by the probe laser. (b) Slow (0.30 eV) electrons generated by the probe laser. The voltage between the parabolic meshes ($U_p=-0.5$ V) is adjusted to maximize the electron signal. The acceleration voltage is $U_a=3.6$ V.

B. Lasers

Coherent radiation with nearly transform-limited bandwidth is provided by pulsed amplification of single-mode cw radiation (see Fig. 2). The probe-laser pulse at 326 nm and the excitation-laser pulse at 250 nm are provided by a pulsed dye amplifier (Quanta Ray PDA), seeded by the output of a single-mode cw dye laser (Coherent 699) operating at 652 nm. The amplifier is pumped by the frequency doubled radiation of an injection seeded pulsed Nd:YAG (yttrium aluminum garnet) laser (Quanta Ray GCR 4). The output of the pulsed dye amplifier is frequency doubled in a BBO crystal to yield radiation at 326 nm, which is mixed with the fundamental frequency of the Nd:YAG laser in a potassium dihydrogen phosphate crystal to obtain radiation at 250 nm with pulse energies up to a few hundred μJ and a pulse duration of 3.4 ns [FWHM (full width at half maximum) of the intensity]. The residual radiation at 326 nm is used as the probe pulse (pulse duration 3.6 ns). The spectral bandwidth of the ultraviolet radiation is about $\Delta\nu=140$ MHz, which is very close to the transform limit $\Delta\nu_{min}=130$ MHz for laser pulses with the given width and a Gaussian temporal profile. A second pulsed dye amplifier, seeded by another cw dye laser system running at 606 nm with a modehop-free tuning range of 30 GHz, provides the dressing-laser pulse with pulse energies up to several mJ and a pulse duration of 5.5 ns. The dressing-laser pulse passes through an optical delay line before it is spatially overlapped with the probe-laser beam axis. The optical delays are adjusted such that the coincident probe and dressing-laser pulses are delayed by 5 ns with respect to the excitation-laser pulse. The laser beams are focused by quartz lenses onto the axis of the atomic beam. The beam diameters (FWHM of intensity) in the interaction region are 140 μm for the probe and 310 μm for the dressing laser. The probe laser is attenuated to intensities typically in

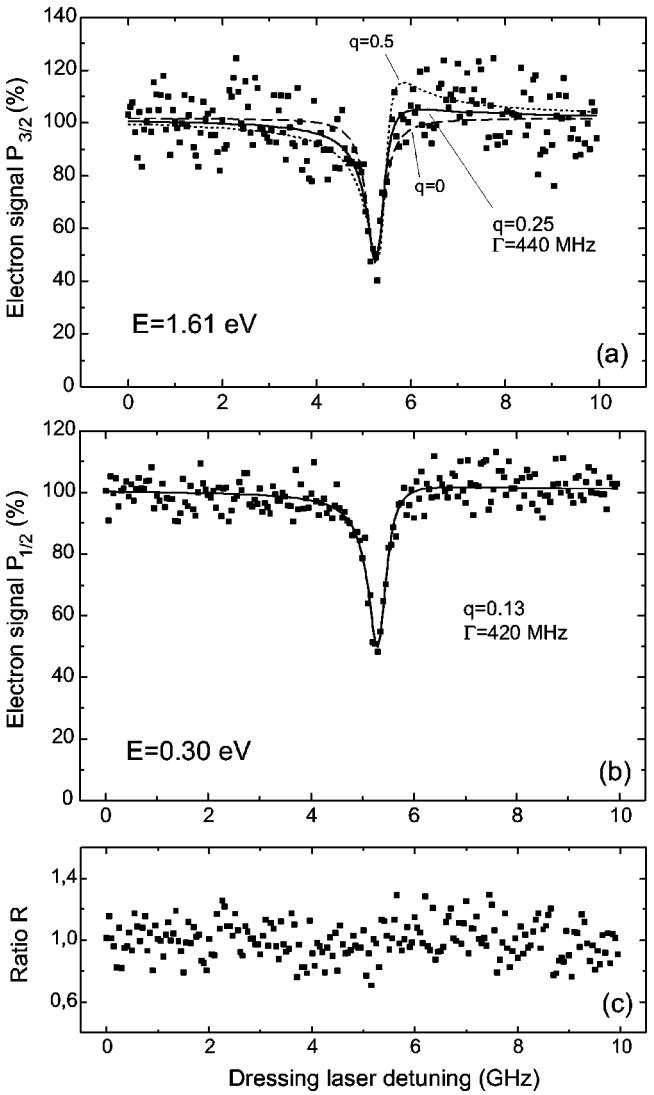

FIG. 4. LICS in the two photoionization continua $^2P_{1/2}$ and $^2P_{3/2}$ of xenon. The signals related to the fast and slow photoelectrons as a function of the dressing detuning are shown. The dressing detuning is defined such that it increases with dressing laser frequency. The signals in both channels far away from the resonance are normalized to 100%. The solid lines are fits to the experimental data. Peak intensities are $I_p=17$ MW/cm^2 and $I_d=380$ MW/cm^2. The shape of the LICS in the two channels is almost identical. (a) Photoelectrons of energy 1.61 eV in the $^2P_{3/2}$ continuum. Besides the fit curve (solid line) we show profiles for $q=0$ (dashed line) and $q=0.5$ (dotted line) for comparison. (b) Photoelectrons of energy 0.30 eV in the $^2P_{1/2}$ continuum. (c) Ratio $R=S(^2P_{3/2})/S(^2P_{1/2})$ of the normalized electron signals from both continua.

the range of a few 10^7 W/cm^2 in order to work in the weak probe-laser regime ($\Gamma_p\tau_p \ll 1$, where Γ_p is the ionization rate induced by the probe laser and τ_p is its pulse duration), as well as to prevent saturation of the electron detection.

For measuring the shift of the spectral position of the LICS (described in Sec. V C) an additonal, independent laser system is used to produce the excitation pulse at 250 nm. The radiation of a multimode, pulsed dye laser (Lambda Physik, LPD 3000, operated with laser dye Coumarin 102 at 500 nm) pumped by an excimer laser (Lambda Physik, LPX 220) is frequency doubled in a BBO crystal to yield 15-ns pulses at 250 nm with energies of several hundred μJ.

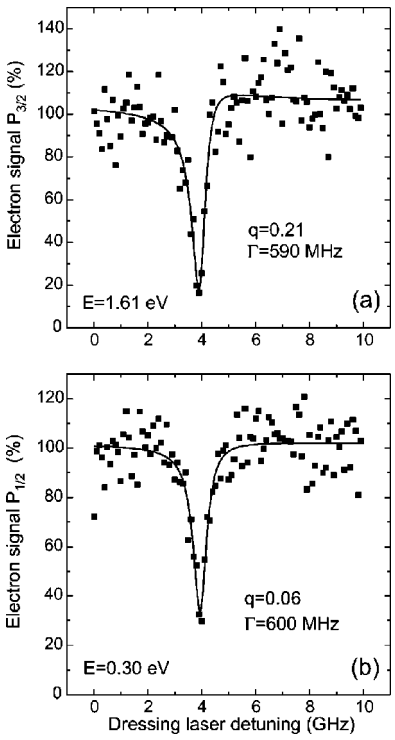

FIG. 5. Same as in Fig. 4, but with $I_p=17$ MW/cm^2, $I_d=680$ MW/cm^2. For higher dressing intensity a more pronounced ionization suppression is achieved.

IV. RESULTS AND DISCUSSION

Figure 4 shows the variation of the signals generated by the fast and slow photoelectrons [$^2P_{3/2}$ continuum, frame (a), and $^2P_{1/2}$ continuum, frame (b), respectively] when the frequency of the dressing laser is tuned across the two-photon resonance between the $5p^5\,6p[1/2]_0$ and the $5p^5\,9p[1/2]_0$ states. The absolute value of the branching ratio cannot be deduced from these data because the energy-dependent transmission function of the spectrometer is not well known. The signal at large detuning from the LICS is normalized to 100% in both channels. Both channels reveal pronounced, spectrally narrow LICS profiles, where the photoelectron signal is reduced to about 50% as compared with the value for large detunings of the dressing-laser frequency from resonance. For higher dressing-laser intensity (see Fig. 5) an ionization suppression up to 80% is observed. The spectral width of the observed features increases accordingly. The line shapes of the LICS were fitted to Fano profiles [2,12,23] $\sigma(x)=\sigma_0+A(x-q)^2/(x^2+1)$, where $x\equiv D/(\Gamma/2)$. The dressing detuning D is defined such that it increases with dressing-laser frequency and the parameter Γ determines the width of the profile. The fit curves along with the parameters q and Γ are given in the figures. All profiles show pronounced suppression but almost no enhancement, which yields a Fano parameter close to $q=0$. At the given signal-to-noise ratio a strict upper limit of $q<0.5$ applies. Figure

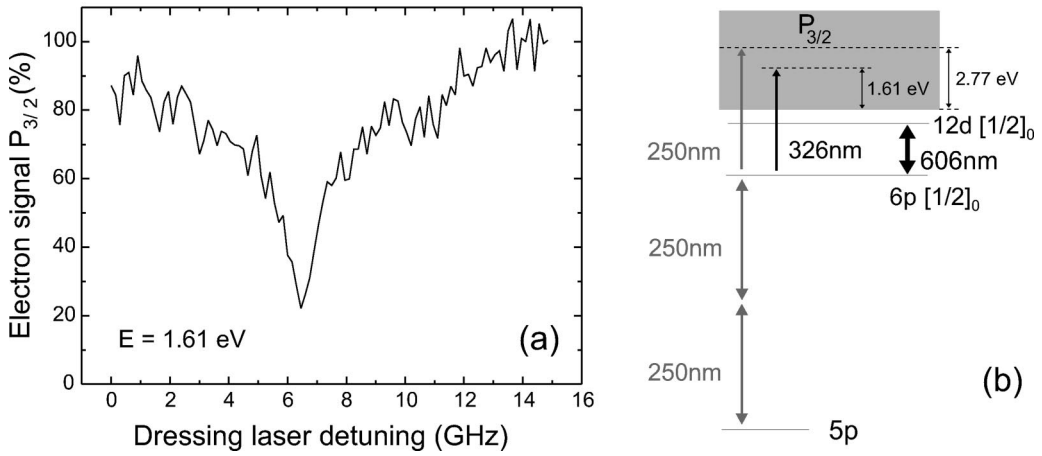

FIG. 6. (a) Dark resonance generated by dressing-laser-induced coupling between the $5p^5\,6p[1/2]_0$ state and the $5p^5 12d[1/2]_1$ Rydberg state for a peak intensity $I_d = 47$ MW/cm^2 and a pulse delay of 5 ns. The population in the $5p^5\,6p[1/2]_0$ state is not completely suppressed because the dark resonance is generated in the wing of the temporal profile of the dressing pulse. The dark resonance was observed at a dressing frequency different from the spectral position of the LICS. The linewidth of the feature ($\approx 2-3$ GHz) is large compared to the observed LICS. This is due to saturation broadening effects on the strong, dressing laser driven one-photon resonance between bound atomic states, while LICS involves weaker, thus less broadened, bound-continuum couplings. (b) The coupling scheme.

4(b) shows, besides the fit curve, profiles for $q=0$ and $q=0.5$ for comparison. We confirmed experimentally that for the intensities applied here the probe-laser ionization is not saturated. Saturation would reduce any enhancement of the ionization rate and would thus mimic a Fano parameter close to zero. Therefore the Fano parameter is indeed $q \approx 0$. This value of q shows that the Rabi frequencies related to the two-photon Raman couplings between the bound states are much smaller than the ionization rates. In most LICS experiments reported so far [5–7,10,11,14,15] LICS profiles with a Fano parameter of order of unity or larger were observed, except for Ref. [19], where the results indicate $q \approx 0$.

The variation of the electron yields for ionization to the two continua with dressing-laser frequency is identical. Within the experimental accuracy the ratio of the electron signals in the two channels [see Fig. 4(c)] is independent of the detuning of the dressing laser. Therefore, control of the branching ratio by laser frequency tuning is not possible. Since this behavior was unexpected we carefully verified experimentally (see Sec. V) that the structures shown in Figs. 4 and 5 are not generated by processes other than LICS. The results presented in Sec. V show unambiguously that the observed structure is indeed LICS.

The reasons for the identical LICS in the two continua is currently investigated theoretically. A detailed quantitative analysis requires an accurate knowledge of the atomic parameters. The ionization amplitudes $g_{ij}^{(\alpha)}$ in Eqs. (1) and (2) are determined by one-photon matrix elements between bound and continuum states. The coefficients $C_i(t)$ are solutions of a system of coupled differential equations, which contain the Fano parameter q [12] of the system and the dynamic Stark shifts. Both quantities are related to two-photon amplitudes involving a sum over bound-bound and bound-continuum matrix elements, the summation extending over all states of the atom. Therefore the bound and continuum wave functions of the system need to be calculated. In xenon this is a very difficult task.

One possible approach is the use of multichannel quantum defect theory (MQDT) [24], which is a well-known tool for the analysis of atomic spectra. It has been applied for calculating the atomic parameters of the rare gases [25], particularly the multiphoton ionization of xenon and krypton [26,27]. For calculating the Fano parameter and the Stark shifts, which are determined by two-photon processes, an approach like the one in Ref. [27] could be used. In that work the polarizability tensor is approximated by limiting the summation to contributions from bound states only. However, a preliminary analysis revealed severe problems. It turned out that the contributions from Rydberg states do not decrease with increasing principal quantum number. This indicates that the contributions from autoionizing states and continuum states must be included in the summation, a task that is not simple in the MQDT formalism [27]. Furthermore, the low-lying $5p^5\,6p[1/2]_0$ state cannot be well described by MQDT, i.e., the calculated ionization amplitudes $g_{1p}^{(\alpha)}$ will not be accurate. Thus, at present, accurate theoretical modeling of LICS in the coupling scheme implemented here is not completed yet. We hope that the reliable experimental data reported in this work will stimulate theoretical work towards overcoming the present limitations.

Here we identify the conditions under which the LICS in the two continua are expected to be identical. The ionization amplitudes $g_{ij}^{(\alpha)}$ determine the line shapes in the individual continua. Our preliminary theoretical results indicate that only two out of the five continuum states, one from the $^2P_{1/2}$ manifold and one from the $^2P_{3/2}$ manifold, contribute to the LICS process. These are the continua $\alpha=1$ and $\alpha=4$ (marked by bold arrows in Fig. 1). In this case an identical normalized line shape in the two ionization channels will occur if the ionization amplitudes for these two continuum states are proportional to each other, i.e., $g_{1p}^{(4)} = a g_{1p}^{(1)}$ and $g_{2d}^{(4)} = a g_{2d}^{(1)}$, where a is a constant.

We like to note, that the coefficients in Eqs. (1) and (2),

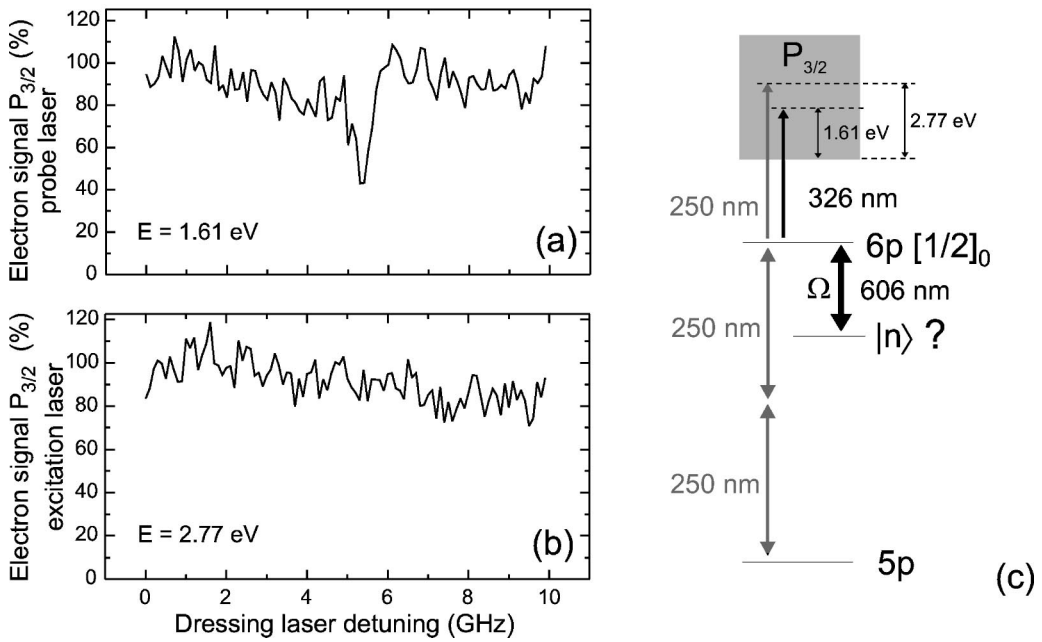

FIG. 7. Exclusion of a dark resonance in the excitation of the $5p^5\,6p[1/2]_0$ state by dressing-laser-induced one-photon or multiphoton coupling to some bound state $|n\rangle$. (a) LICS in the probe-laser-induced electron signal. (b) The electron signal induced by the excitation laser, which monitors the population in the $5p^5\,6p[1/2]_0$ state, does not show a minimum at the spectral position of the LICS. (c) The coupling scheme.

and therefore the profile and modulation depth of the LICS depend strongly upon the polarization of the interacting laser pulses. The most obvious choice, as implemented in our experimental setup, is to have all laser pulses being linearly polarized parallel to each other. Indeed, we confirmed in the experiment that the LICS completely vanishes, if the polarizations of the probe and dressing laser pulse are perpendicular to each other.

V. EXPERIMENTAL VERIFICATION OF THE LICS

In this section we discuss other processes that could lead to a suppression of the ionization signal, such as trapped state formation by coupling of bound states or multiphoton ionization into channels that are not detected. We demonstrate experimentally that such processes are not responsible for the observed suppression of ionization.

A. Consequences of dark resonance formation

One of the mechanisms that could decrease the rate of excitation to the $5p^5\,6p[1/2]_0$ state (and thus reduce the ionization yield) is the formation of a dark resonance due to coherent coupling between the $5p^5\,6p[1/2]_0$ state and another bound state induced by the dressing-laser field (coherent population trapping [28,29]). In this process, which is closely related to electromagnetically induced transparency [30,31], the populated initial state (state 1) is coupled to an excited intermediate state (state 2) by a weak excitation-laser field (usually named ''probe laser'' in the literature; here we use the term ''excitation laser'' in order to avoid confusion with the probe laser in the LICS experiment). The intermediate state is coupled to another bound state (state 3) by a strong dressing-laser field. Without the dressing laser the intermediate state is populated by the excitation laser. The transfer of population from the initial to the intermediate state is inhibited when the dressing laser is switched on and its frequency is tuned to resonance with the transition between states 2 and 3 [28,29]. We have verified, as shown below, that the dressing laser (which couples the $5p^5\,9p[1/2]_0$ state to the continuum) does not induce additional couplings to bound states, which prevent the population of the $5p^5\,6p[1/2]_0$ state by coherent population trapping.

1. Consequences of dark resonances induced by one-photon coupling to Rydberg states

In the coupling scheme shown in Fig. 1 the dressing laser may couple the $5p^5\,6p[1/2]_0$ state to ns/nd Rydberg states with $n>10$. The corresponding dark resonances, which are most pronounced for coincident excitation and dressing-laser pulses, were observed and analyzed in detail in Ref. [29]. For the pulse sequence used in the LICS experiment, where the dressing laser is delayed by 5 ns with respect to the excitation pulse, the pulses only partially overlap in time. Even with only partial overlap a reduction of the ion yield is still observable. In Fig. 6 we show the dark resonance whose spectral position is closest to the expected frequency for the LICS. It is generated by coupling the $5p^5\,6p[1/2]_0$ level to the $5p^5\,12d[1/2]_1$ Rydberg state. This dark resonance was observed at a dressing wavelength $\lambda_d=606.1590$ nm. In the same experimental configuration the LICS was observed at $\lambda_d=606.1080$ nm with an uncertainty of ± 0.0002 nm. Therefore, a dark resonance induced by coupling to Rydberg states is *not* the cause for the structures shown in Figs. 4 and 5.

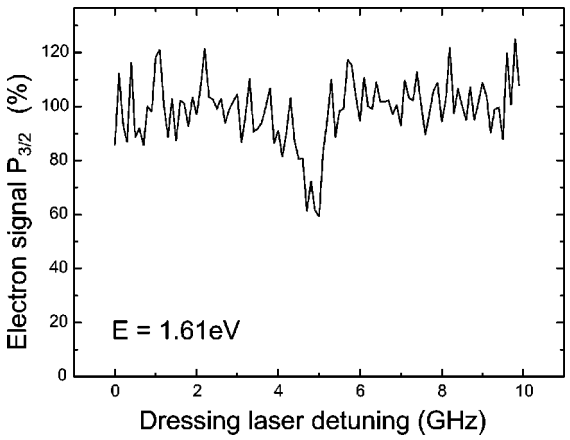

FIG. 8. Exclusion of a dark resonance in the excitation of the $5p^5\,6p[1/2]_0$ state by dressing-laser-induced one-photon or multiphoton coupling to some bound state $|n\rangle$. The LICS was still observed for a pulse delay of 40 ns, where excitation pulse (15 ns) and dressing pulse (5.5 ns) were completely separated in time. In this experiment the excitation pulse was generated by the excimer-pumped dye laser (see Sec. III B).

2. Exclusion of dark resonances induced by one-photon or multiphoton coupling to other bound states

We also verified that the structures are not caused by a dark resonance induced by one-photon or multiphoton coupling to any other bound state. The population in the $5p^5\,6p[1/2]_0$ state was monitored while tuning the dressing frequency across the spectral position of the LICS. Figure 7(a) shows, as expected, the LICS in the electron signal (1.61 eV) generated by the probe laser. The electron signal generated by the excitation laser (2.77 eV) [see Fig. 7(b)] is a measure of the population in the $5p^5\,6p[1/2]_0$ state. Any dark resonance formation due to the coupling of the $5p^5\,6p[1/2]_0$ state to another bound level by the dressing laser would reduce the excitation of the $5p^5\,6p[1/2]_0$ level from the bound state and thus reduce the electron yield at 2.77 eV. This signal does *not* show a minimum at the spectral position of the LICS.

Furthermore, a dressing-laser-induced dark resonance in the excitation of the $5p^5\,6p[1/2]_0$ state can only occur when the excitation and dressing pulses overlap at least partially in time. Figure 8 displays the electron signal (1.61 eV) for a pulse delay of 40 ns. Although the excitation pulse (15 ns) and the dressing pulse (5.5 ns) do not overlap in time, and thus the two lasers cannot lead to a dark resonance, the LICS is observed. Therefore a dark resonance does not cause the ionization suppression displayed in Figs. 4 and 5.

B. Consequences of a depletion of the $5p^5\,6p[1/2]_0$ state by resonant two-photon ionization induced by the dressing laser

The $5p^5\,6p[1/2]_0$ state may also be ionized by nonresonant two-photon ionization induced by the dressing laser. This means that the dressing laser and the probe laser compete for the population in the $5p^5\,6p[1/2]_0$ state; an efficient multiphoton ionization by the dressing laser will reduce the electron signals at 1.61 eV and 0.30 eV induced by the probe laser. The ionization by the dressing laser may be resonantly enhanced when the dressing frequency is tuned to the one-photon resonance between the $5p^5\,6p[1/2]_0$ state and another bound state $|n\rangle$ [see Fig. 9(c)]. The enhanced ionization would cause a more pronounced depletion of the $5p^5\,6p[1/2]_0$ state and therefore a decrease in the probe-laser-induced electron signal. We verified that this effect is not responsible for the structures in Figs. 4 and 5. The electron signal (1.89 eV) induced by the dressing laser was monitored [see Fig. 9(b)] while tuning the dressing fre-

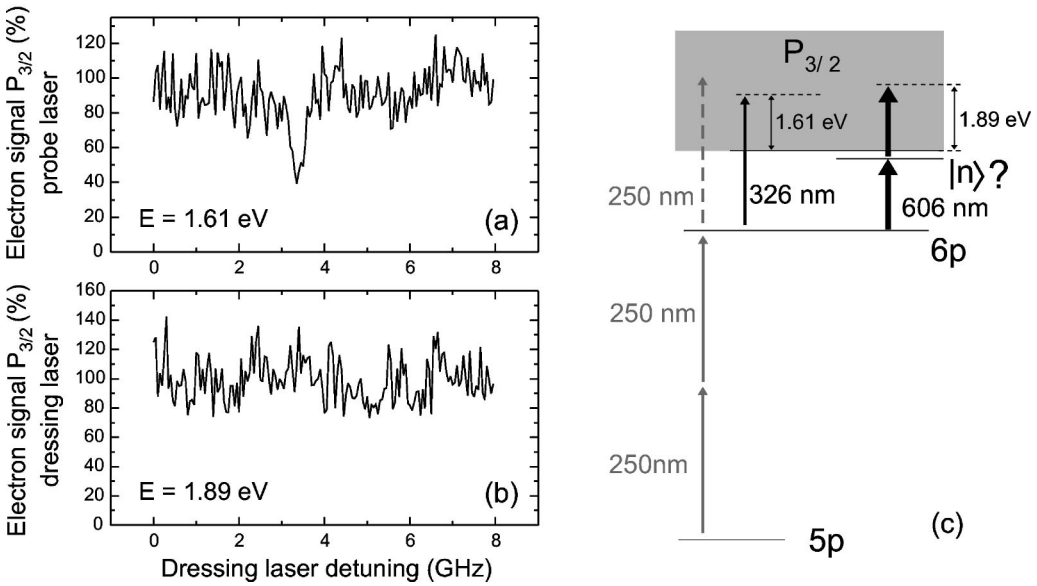

FIG. 9. Exclusion of a resonant enhancement in the dressing-laser-induced two-photon ionization of the $5p^5\,6p[1/2]_0$ state. (a) LICS in the probe-laser-induced electron signal. (b) The dressing-laser-induced electron signal is *not* enhanced when the dressing frequency is tuned across the spectral position of the LICS. (c) The coupling scheme.

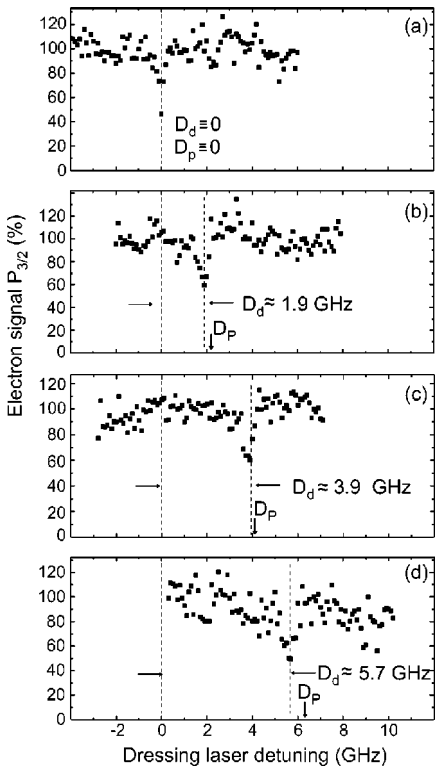

FIG. 10. Variation of the spectral position of the LICS with the probe-laser frequency. The electron signal from the $2P_{3/2}$ continuum is measured as a function of the dressing detuning for four different frequencies of the probe laser. The frequencies of the probe and dressing laser for which the LICS is observed in (a) are defined as ν_p^0 and ν_d^0. In (b)–(d) the frequency ν_p of the probe laser is set to three different values as indicated by the detuning $D_p \equiv \nu_p - \nu_p^0$, marked by vertical arrows on the frequency axis. The dressing frequency is tuned across the minimum. The detuning $D_d \equiv \nu_d - \nu_d^0$ is determined from the spectral position ν_d of the minimum. As expected for LICS both detunings are shifted, within the experimental accuracy, by the same value. The LICS in the data shown here is not as pronounced as in Figs. 4 and 5 due to larger pulse energy fluctuations and time jitter in the laser setup used here (see text).

quency across the spectral position of the LICS. The signal at 1.89 eV does *not* show an enhancement at the dressing frequency where the LICS in the probe-laser-induced electron signal (1.61 eV) [see Fig. 9(a)] is observed.

C. Shift of the spectral position of the LICS

As a final test we examined the variation of the spectral position of the LICS with the probe-laser frequency. In the experimental setup shown in Fig. 2 an independent variation of the probe-laser frequency is not possible because the probe radiation at 326 nm and the excitation radiation at 250 nm are generated from the fundamental at 652 nm by nonlinear frequency mixing. A variation of the probe frequency requires the tuning of the fundamental frequency, which changes the frequency of the excitation laser. The maximum probe-laser detuning is limited by the linewidth of the $5p^6\,{}^1S_0 \rightarrow 5p^5\,6p[1/2]_0$ transition. Wider tunability for the probe frequency is achieved by generating the excitation pulse at 250 nm in an independent laser system as described in the last paragraph of Sec. III B. The signal-to-noise ratio is reduced in this configuration due to larger pulse-to-pulse fluctuations of the pulse energy of the excitation laser and the delay between the excitation- and probe-laser pulses.

It is an experimental signature expected for LICS, which is generated by a two-photon process, that the dressing-laser frequency at which the two-photon resonance occurs varies linearly with the probe-laser frequency (see the coupling scheme in Fig. 1). If, however, the structure were caused by one of the effects discussed in Secs. V A and V B it would occur at a fixed dressing-laser frequency independent of the frequency of the probe laser. Figure 10 shows indeed that the dressing frequency at which the LICS is observed varies linearly with the probe-laser frequency.

VI. CONCLUSION

We observed pronounced, spectrally narrow LICS in both photoionization channels of xenon. A suppression of the electron signal up to 80% was achieved. The line shape of the signal yields a Fano parameter of $q < 0.5$. Attempts to reproduce the experimental data by a calculation based on MQDT failed. The results of calculations of two-photon matrix elements do not converge when an increasing number of intermediate Rydberg states is included in the summation. Therefore inclusion of autoionizing and continuum states in the calculation seems necessary. However, the theoretical framework has not yet been developed. In a series of experiments we verified that the observed structures are indeed LICS. No enhancement was observed, which indicates weak Raman-type coupling as compared to the ionization rates. Although the LICS is well pronounced for both continua, control of the branching ratio for ionization into the two continua by dressing-laser detuning is not possible since in this coupling scheme the LICS is identical for both continua.

ACKNOWLEDGMENTS

We acknowledge support from the Deutsche Forschungsgemeinschaft under Be 623/34 and 436 UKR 113/46/2-1, as well as from INTAS (99-00019), and from the German-Israeli Foundation (1-644-118.5/1999). This work was supported in part by the European Community's Human Potential Program under Contract No. HPRN-CT-1999-00129, COCOMO. L.P.Y. and K. Bergmann acknowledge support through a NATO collaborative research grant. We thank H. Hotop and B. W. Shore for valuable discussions.

[1] P. E. Coleman, P. L. Knight, and K. Burnett, Opt. Commun. **42**, 171 (1982).
[2] P. L. Knight, M. A. Lauder, and B. J. Dalton, Phys. Rep. **190**, 1 (1990).
[3] Y. I. Heller and A. K. Popov, Kvant. Elektron. (Moscow) **3**, 1129 (1976) [Sov. J. Quantum Electron. **6**, 606 (1976)].
[4] Bo-nian Dai and P. Lambropoulos, Phys. Rev. A **36**, 5205 (1987); **39**, 3704 (1989).
[5] Y. I. Heller, V. F. Lykinykh, A. K. Popov, and V. V. Slabko, Phys. Lett. **82A**, 4 (1981).
[6] L. I. Pavlov, S. S. Dimov, D. I. Metchkov, G. M. Mileva, K. V. Stamenov, and G. B. Altshuller, Phys. Lett. **89A**, 441 (1982); S. S. Dimov, L. I. Pavlov, K. V. Stamenov, Y. I. Heller, and A. K. Popov, Appl. Phys. B **30**, 35 (1983).
[7] M. H. R. Hutchinson and K. M. M. Ness, Phys. Rev. Lett. **60**, 105 (1988).
[8] X. Tang, A. l'Huillier, and P. Lambropoulos, Phys. Rev. Lett. **62**, 111 (1989).
[9] Y. L. Shao, D. Charalambidis, C. Fotakis, Jian Zhang, and P. Lambropoulos, Phys. Rev. Lett. **67**, 3669 (1991); S. Cavalieri, F. S. Pavone, and M. Matera, *ibid.* **67**, 3673 (1991).
[10] S. Cavalieri, M. Matera, F. S. Pavone, Jian Zhang, P. Lambropoulos, and T. Nakajima, Phys. Rev. A **47**, 4219 (1993); S. Cavalieri, R. Eramo, and L. Fini, J. Phys. B **28**, 1793 (1995); R. Eramo, S. Cavalieri, L. Fini, M. Matera, and L. F. DiMauro, *ibid.* **30**, 3789 (1997).
[11] T. Halfmann, L. P. Yatsenko, M. Shapiro, B. W. Shore, and K. Bergmann, Phys. Rev. A **58**, R46 (1998).
[12] L. P. Yatsenko, T. Halfmann, B. W. Shore, and K. Bergmann, Phys. Rev. A **59**, 2926 (1999).
[13] T. Halfmann, J. Koensgen, and K. Bergmann, Meas. Sci. Technol. **11**, 1510 (2000).
[14] O. Faucher, D. Charalambidis, C. Fotakis, Jian Zhang, and P. Lambropoulos, Phys. Rev. Lett. **70**, 3004 (1993); O. Faucher, Y. L. Shao, and D. Charalambidis, J. Phys. B **26**, L309 (1993); O. Faucher, Y. L. Shao, D. Charalambidis, and C. Fotakis, Phys. Rev. A **50**, 641 (1994).
[15] N. E. Karapanagioti, O. Faucher, Y. L. Shao, D. Charalambidis, H. Bachau, and E. Cormier, Phys. Rev. Lett. **13**, 2431 (1995); N. E. Karapanagioti, D. Charalambidis, C. J. G. J. Uiterwaal, C. Fotakis, H. Bachau, I. Sanchez, and E. Cormier, Phys. Rev. A **53**, 2587 (1996); H. Bachau and I. Sanchez, Z. Phys. D: At., Mol. Clusters **38**, 19 (1996).
[16] O. Faucher, E. Hertz, B. Lavorel, D. Charalambidis, R. Chaux, and H. Berger, J. Phys. B **32**, 4485 (1999).
[17] Z. Chen, M. Shapiro, and P. Brumer, Chem. Phys. Lett. **228**, 289 (1994); P. Brumer, Z. Chen, and M. Shapiro, Isr. J. Chem. **34**, 137 (1994).
[18] A. Shnitman, I. Sofer, I. Golub, A. Yogev, M. Shapiro, Z. Chen, and P. Brumer, Phys. Rev. Lett. **76**, 2886 (1996).
[19] S. Cavalieri, R. Eramo, L. Fini, M. Materazzi, O. Faucher, and D. Charalambidis, Phys. Rev. A **57**, 2915 (1998).
[20] R. Eramo and S. Cavalieri, Opt. Commun. **149**, 296 (1998).
[21] D. J. Trevor, L. D. Van Woerkom, and R. R. Freeman, Rev. Sci. Instrum. **60**, 1051 (1989).
[22] J. Steadman and J. A. Syage, Rev. Sci. Instrum. **64**, 3094 (1993).
[23] U. Fano, Phys. Rev. **124**, 1866 (1961).
[24] M. J. Seaton, Proc. Phys. Soc. London **88**, 801 (1966); K. T. Lu and U. Fano, Phys. Rev. A **2**, 81 (1970); U. Fano, *ibid.* **2**, 353 (1970); M. J. Seaton, Rep. Prog. Phys. **46**, 167 (1983).
[25] K. T. Lu, Phys. Rev. A **4**, 579 (1971); A. F. Starace, J. Phys. B: Atom Mol. Phys. **6**, 76 (1973); J. Geiger, Z. Phys. A **282**, 129 (1977); M. Aymar, O. Robaux, and C. Thomas, J. Phys. B **14**, 4255 (1981).
[26] P. Gangopadhyay, X. Tang, P. Lambropoulos, and R. Shakeshalf, Phys. Rev. A **34**, 2998 (1986); P. R. Blazewich, X. Tang, R. N. Compton, and J. A. D. Stockdale, J. Opt. Soc. Am. B **4**, 770 (1987); X. Tang, A. L'Huillier, and P. Lambropoulos, Phys. Rev. Lett. **62**, 111 (1989); S. J. Bajic, R. N. Compton, X. Tang, and P. Lambropoulos, Phys. Rev. A **44**, 2102 (1991).
[27] A. L'Huillier, X. Tang, and P. Lambropoulos, Phys. Rev. A **39**, 1112 (1989).
[28] E. Arimondo, Prog. Opt. **35**, 259 (1996).
[29] T. Halfmann, K. Böhmer, L. P. Yatsenko, and K. Bergmann, Eur. Phys. J. D **17**, 113 (2001).
[30] S. E. Harris, Phys. Today **50**, 36 (1997).
[31] J. P. Marangos, J. Mod. Opt. **45**, 471 (1998).